CARBON letters

Original Articles
Carbon Letters Vol. 27, 64-71 (2018)

Anatase TiO_2-doped activated carbon fibers prepared by ultrasonication and their capacitive deionization characteristics

Da Hee Kang, Hanjoo Jo, Min-Jung Jung, Kyoung Hoon Kim and Young-Seak Lee*

Department of Chemical Engineering and Applied Chemistry, Chungnam National University, Daejeon 34134, Korea

Article Info

Received 9 August 2017
Accepted 19 December 2017

***Corresponding Author**
E-mail: youngslee@cnu.ac.kr
Tel: +82-42-821-7007

Open Access
DOI: http://dx.doi.org/10.5714/CL.2018.27.064

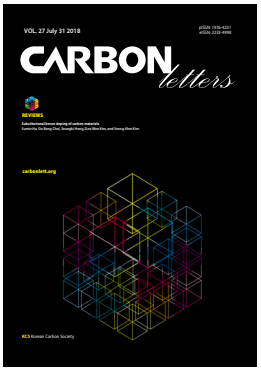

http://carbonlett.org

pISSN: 1976-4251
eISSN: 2233-4998

Abstract

TiO_2-doped activated carbon fibers (ACFs) were successfully prepared as capacitive deionization (CDI) electrode materials by facile ultrasonication-assisted process. ACFs were treated with titanium isopropoxide (TTIP) and isopropyl alcohol solutions of different concentrations and then calcinated by ultrasonication without heat-treatment. The results show that a certain amount of anatase TiO_2 was present on the ACF surface. The specific capacitance of the TiO_2-doped ACF electrode was remarkably improved (by 93.8% at scan rate of 50 mV s^{-1}) over that of the untreated ACF electrode, despite decreases in the specific surface area and total pore volume upon TiO_2 doping. From the CDI experiments, the salt adsorption capacity and charge efficiency of the sample with TTIP percent concentration of 15% were found to considerably increase by 71.9 and 57.1%, respectively. These increases are attributed to the improved wettability of the electrode, which increases the number of surface active sites and facilitates salt ion diffusion in the ACF pores. Additionally, the Ti-OH groups of TiO_2 act as electrosorption sites, which increases the electrosorption capacity.

Key words: TiO_2, activated carbon fiber, capacitive deionization, ultrasonication

1. Introduction

Capacitive deionization (CDI) is an emerging technology that has the advantages of low energy consumption, relatively inexpensive operation, simple regeneration, and no secondary contamination [1]. CDI is based on the electrosorption of ions through the formation of an electrical double-layer on the surface of a porous material. When the electrode pair are charged with a voltage of approximately 1 V, salt ions are electrostatically removed from the feed water forming the electrical double-layer [2-4].

Carbon materials are considered to be the most promising materials for CDI applications because of their high specific surface area, good conductivity, and chemical and electrochemical stability [5]. In particular, activated carbon fibers (ACFs) have been studied as CDI electrode materials due to their short ion diffusion paths, uniform pore size, and good conductivity [6]. Theoretically, as the specific surface area of a carbon material increases, its capability of accumulating salt ions increases [7]. However, the CDI performance does not necessarily increase proportionally with the specific surface area of the porous carbon but rather is affected by both the specific surface area and the surface properties. Therefore, surface modification of carbon materials is important to improve CDI performance.

Various surface modification methods have been investigated, such as treatment with acid/base solutions and the addition of organic/inorganic materials. Among these methods, the introduction of metal oxides has the advantages of low cost, ecofriendliness, good chemical stability, and high capacitance [8,9]. In this respect, carbon materials modified with TiO_2 have been reported as CDI electrode materials [10-13]. TiO_2 is hydrophilic due to the presence of hydroxyl groups on its surface. The improved wettability of an electrode by TiO_2 increases the number of active sites on the surface and facilitates ion diffusion, which benefits the CDI performance [14-16].

TiO_2/carbon material composites are mainly prepared by sol-gel methods. In the conventional sol-gel method, high temperature (above 500°C) and a long calcination time (over 2 h) are required to induce crystallization. In addition, this calcination process must be conducted in inert or vacuum conditions [17]. Such processes consume a large amount of energy, and the cost restricts the application of TiO_2/carbon materials in CDI. Thus, it is necessary to develop a facile sol-gel method to prepare TiO_2/carbon material composites without heat-treatment.

The application of ultrasound in the synthesis of TiO_2 has become a useful method in recent years. When solutions are exposed to strong ultrasound irradiation, bubbles are implosively collapsed by acoustic fields in the solution. High-temperature and high-pressure fields are produced at the centers of the bubbles, which is known as acoustic cavitation [18]. This method rapidly forms high-purity TiO_2 nanoparticles with a narrow size distribution [19].

In this study, a facile ultrasonication-assisted process is suggested as a new and energy-efficient process for quickly preparing TiO_2-doped ACFs without heat-treatment, and the prepared TiO_2-doped ACFs were used as an electrode material for CDI. In addition, the effect of the introduction of TiO_2 on the electrochemical properties was investigated.

2. Experimental

2.1. Preparation of TiO_2-doped ACFs

Pitch-based ACFs (A-10, Osaka Gas Co., Japan), as the active material, and titanium isopropoxide (TTIP; 97%, Aldrich, USA), as the TiO_2 precursor, were used in this study. Isopropyl alcohol (IPA; 99.5%, Samchun Pure Chemical Co., Ltd., Korea) was used as the solvent.

The flow chart of the facile ultrasonication-assisted process is shown in Fig. 1. TTIP and IPA were mixed at various concentrations, in which the total volume of the solutions was 20 mL. Then, 5 g of the ACFs was mixed with each solution and stirred for 1 h at room temperature. The treated ACFs were dried for 12 h at 100°C to remove the solvent. The dried samples were calcinated by ultrasonication at room temperature for 40 min. When ultrasound wave was injected into water, cavitation bubbles were formed from pre-existing impurities. Positive and negative pressure were exerted by alternating compression and expansion cycles of ultrasonic waves, respectively. The cavitation bubbles accumulate ultrasonic energy while growing over a few cycles by entrapping the vapor before collapsing [20].

Table 1. Manufacturing conditions for the preparation of TiO_2-doped ACFs

Sample	TTIP (mL)	IPA (mL)
ACF-RAW	-	-
ACF-T05	1.0	19.0
ACF-T15	3.0	17.0
ACF-T25	5.0	15.0

The untreated ACF sample is denoted ACF-RAW. The TTIP-treated ACF samples are denoted ACF-T05, ACF-T15, and ACF-T25, depending on the percent concentration of TTIP. The treatment conditions of the prepared samples and the sample notations are listed in Table 1.

2.2. Characterization of TiO_2-doped ACFs

The morphology of the prepared samples was observed using a high-resolution scanning electron microscope (HR-SEM; SU8230, Hitachi, Japan). The crystallinity of the prepared samples was characterized using an X-ray diffractometer (XRD; D8 Discover, Bruker AXS, Germany) equipped with Cu Kα radiation. The thermal characteristics of the samples were estimated via thermogravimetric analysis (TGA) using a thermal analyzer (SDT Q600, Mettler Toledo, Korea) in air at a heating rate of 10°C/min [21]. The textural properties of the samples were analyzed via a conventional volumetric technique at 77 K using an ASAP 2020 (Micromeritics, USA). The specific surface areas and pore size distributions of the samples were calculated by Brunauer-Emmett-Teller and density functional theory (DFT) equations, respectively.

2.3. Fabrication of the electrodes

The ACFs or TiO_2-doped ACFs, with carbon black (Super P Li, Timcal Ltd., Switzerland) as a conducting agent and poly(vinylidene fluoride) (PVDF; Aldrich) as a binder (8:1:1 mass ratio), were mixed in N-methyl-2-pyrrolidone (NMP; Aldrich) for 6 h to form a slurry. A doctor blade was used to coat the slurry on a graphite sheet using to a wet thickness of 200 μm;

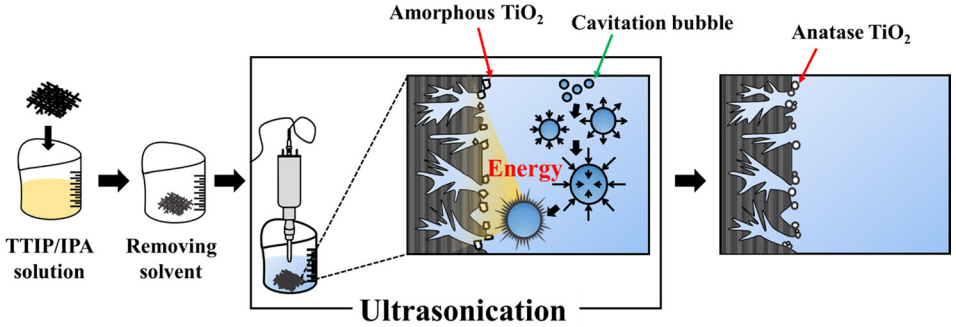

Fig. 1. Preparation of TiO_2-doped ACFs via facile ultrasonication-assisted process.

slurry was then dried at 100°C for 12 h to the remove solvent. The CDI and cyclic voltammetry (CV) electrodes had areas of 90×90 mm^2 and 30×30 mm^2, respectively.

2.4. Characterization of the electrodes

The wettability of the prepared samples was evaluated by a contact angle analyzer (Phoenix 300, Surface Electro Optics Co., Ltd., Korea) [22]. To examine the electrochemical properties of the prepared electrodes, CV was performed using a computer-controlled potentiostat/galvanostat (Ivium Technologies, the Netherlands) using a three-electrode assembly in 1 M NaCl. The fabricated electrodes were used as the working electrode. A platinum plate and Ag/AgCl were used as the counter electrode and the reference electrode, respectively. CV measurement was performed over a potential range of 0–1 V at scan rates of 5 and 50 mV s^{-1} [7]. In addition, electrochemical impedance spectroscopy measurements were taken at 0 V with a potential amplitude of 5 mV in the frequency range of 150 kHz to 0.01 Hz in 1M NaCl solution.

2.5. CDI experiments

The desalination performance of the fabricated electrodes was investigated in a continuous recycling system that included a peristaltic pump (LEPP 150F, Lab SciTech, USA), a conductivity meter (CCT-3300 series, Hebei Create Instrumentation Technologies Co., Ltd., China), and a computer-controlled potentiostat/galvanostat. An NaCl solution with an initial concentration of 500 ppm was pumped into the CDI cell, and the effluent was returned to the unit cell at a flow rate of 20 mL min^{-1}. Upon applying 1.2 V to the CDI cell, a conductivity meter was used to measure the variation in the NaCl conductivity according to its relationship with the concentration at the outlet of the unit cell.

3. Results and Discussion

3.1. Characterization of TiO_2-doped ACFs

Fig. 2 shows HR-SEM images of the surface morphologies of the untreated ACFs and TiO_2-doped ACFs. In Fig. 2 a, the ACFs were shown to have fibrous forms with diameters of 14 μm. In Fig. 2b-d, TiO_2 particles are shown to be randomly distributed on the ACF surface. In addition, the TiO_2 doping amount increased with increases in the TTIP concentration. The TiO_2 particles have nanoflake form with 0.3–0.4 μm. With the TiO_2 doping amount increased, the surface of the TiO_2/ACF samples became rough and some agglomeration was observed.

Fig. 3 exhibits the TGA results of the prepared samples, which were used to confirm TiO_2 doping amount on the ACF surface. Because carbon in the ACFs is completely decomposed in air flow, the weight of TiO_2 can be determined from the remaining weight of the sample [23]. The weight loss at 25–100°C is attributed to the dehydration of physically adsorbed water. The TiO_2-doped ACFs showed a larger drop in weight than did the untreated ACFs, which can be ascribed to interactions between the Ti-O groups in TiO_2 and the OH groups in water, as these interactions increased the content of water in the samples [24].

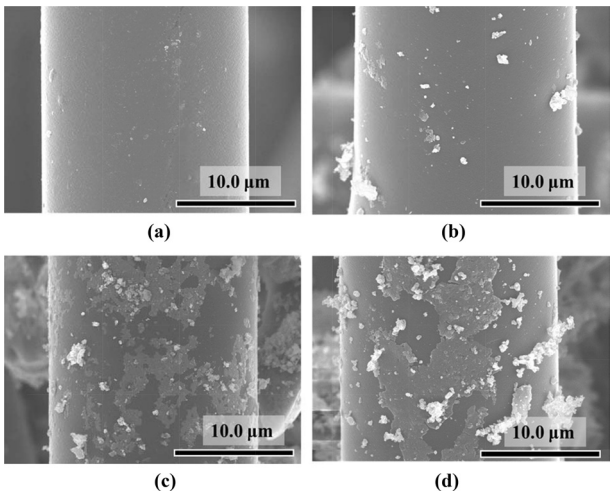

Fig. 2. HR-SEM images of ACF-RAW (a), ACF-T05 (b), ACF-T15 (c), and ACF-T25 (d).

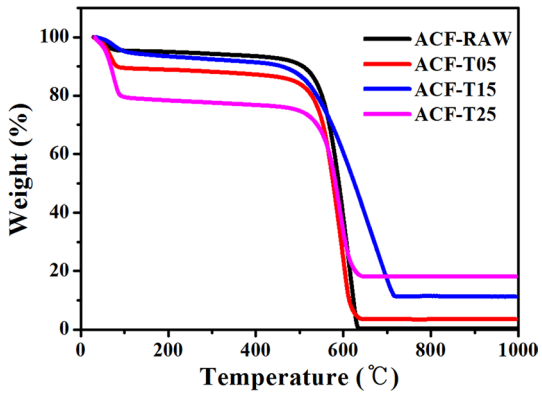

Fig. 3. TGA curves of untreated and TiO_2-doped ACFs.

In addition, the sharp decline at approximately 500°C is due to decomposition of the ACFs [25]. The remaining weights of ACF-RAW, ACF-T05, ACF-T15, and ACF-T25 after carbon decomposition were 0.38, 3.49, 11.20, and 18.11%. Accordingly, the TiO_2 doping amounts of ACF-T05, ACF-T15, and ACF-T25 were determined to be 3.11, 10.82, and 17.73%, respectively. Thus, the amount of TiO_2 doped on the ACF surface can be simply controlled by adjusting the TTIP concentration.

Fig. 4 presents XRD patterns of the untreated ACFs and TiO_2-doped ACFs. In the ACF-RAW pattern, broad diffraction peaks were observed at 26 and 44°; these corresponded to the (100) and (002) planes of graphite (PDF card 41-1487, JCPDS) [26]. The diffraction peak at 26° becomes gradually sharper with increasing TTIP concentration; this is attributed to overlap of the peak corresponding to the (002) plane of amorphous graphite with that corresponding to the (101) plane of anatase TiO_2 [27]. Accordingly, this result implied that the TiO_2 doping amount in the prepared samples increased with increasing TTIP concentration. Additionally, in the ACF-T25 pattern, the diffraction peaks correspond to the (101), (004), (200), (105), (211), and (204) planes of the anatase TiO_2 phase (PDF card 21-1272, JCPDS)

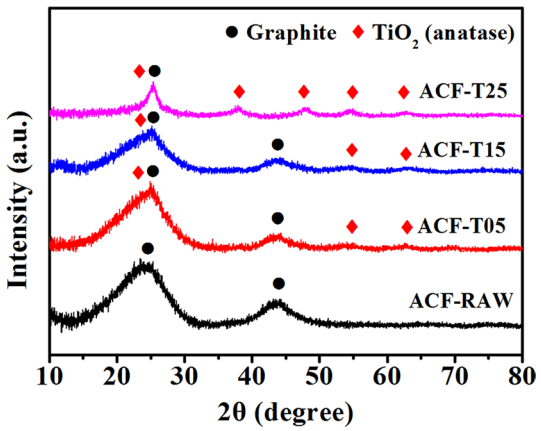

Fig. 4. XRD peaks of untreated and TiO_2-doped ACFs.

[28]. Therefore, TiO_2 precursor was successfully transformed into anatase TiO_2 particles by only the ultrasonication calcining process at room temperature without heat-treatment.

3.2. Textural properties of TiO_2-doped ACFs

Nitrogen adsorption analysis at 77 K was performed to investigate the changes in the textural properties of the prepared samples. As shown in Fig. 5a, ACF-RAW and ACF-T05 have type 1 profiles according to the IUPAC classification. The adsorption steeply increases below a P/P_0 ratio of 0.1 and does not significantly increase beyond that, indicating that the samples were microporous [29]. ACF-T15 and ACF-T25 exhibited hybrid type 1 and type 4 profiles. The amount of adsorption slightly increased below a P/P_0 ratio of 0.1, and gradually increased at greater ratios. Additionally, weak hysteresis loops were observed in the isotherms. These results indicate that ACF-T15 and ACF-T25 are microporous materials with small amounts of mesopores [30]. To examine the change in the pore structure after TiO_2 doping, DFT calculations of the pore size distribution were performed and are shown in Fig. 5b. The fraction of micropores significantly decreased with increased TiO_2 doping because the TiO_2 particles blocked the ACF pores, whereas the fraction of mesopores increased with increased TiO_2 doping. It is thought that the TiO_2 particles doped on the ACF surface formed voids while being aggregated [31]. Table 2 contains detailed information of the textural properties of the prepared samples. The specific surface area and total pore volume of

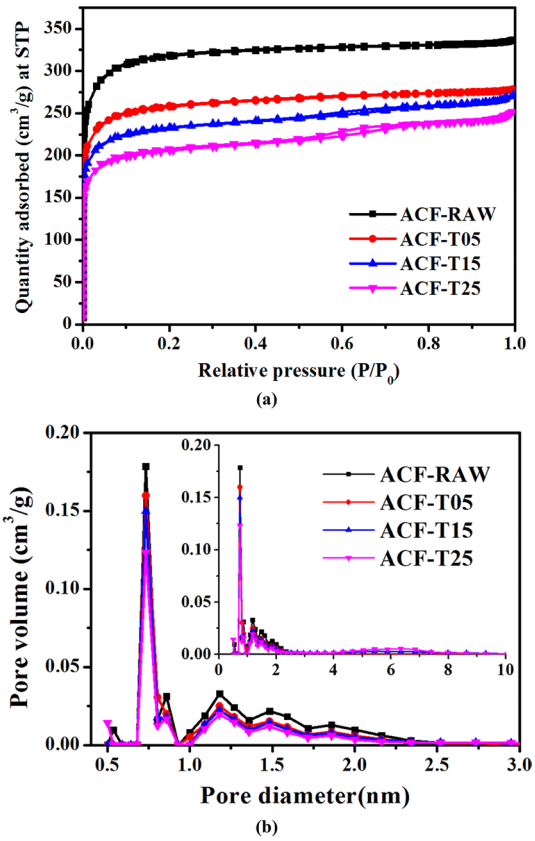

Fig. 5. (a) Nitrogen adsorption isotherms at 77 K and (b) DFT-calculated pore size distribution of untreated and TiO_2-doped ACFs.

the samples decreased with increased TiO_2 doping. The micropore volume also decreased after TiO_2 doping due to TiO_2 particles blocking the ACF pores, which is consistent with the aforementioned results. The mesopore volumes of ACF-T15 and ACF-T25 were larger than that of ACF-T05 due to the formation of voids resulting from aggregation of the TiO_2 particles [31].

Therefore, small TiO_2 particles (approximately 5 μm in diameter) were introduced on the ACF surface via the suggested process. This result was obtained because H_2O was not added during the gelation process, unlike in the conventional sol-gel process. Therefore, this facile ultrasonication-assisted process is a superior process to introduce TiO_2 particles without a major decrease in the specific surface area.

Table 2. Textural properties of untreated and TiO_2-doped ACFs

Sample	Specific surface area ($m^2\ g^{-1}$)	Total pore volume ($cm^3\ g^{-1}$)	Micropore volume ($cm^3\ g^{-1}$)	Mesopore volume ($cm^3\ g^{-1}$)
ACF-RAW	1221.2	0.52	0.49	0.03
ACF-T05	982.8	0.43	0.42	0.01
ACF-T15	886.1	0.43	0.38	0.05
ACF-T25	781.3	0.39	0.34	0.05

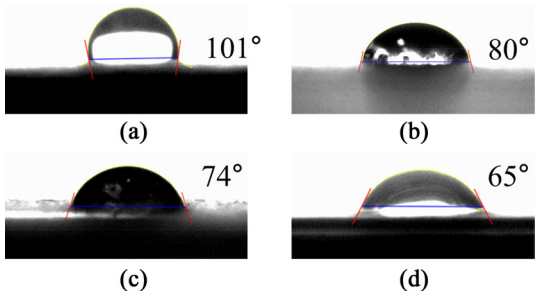

Fig. 6. Images of contact angle measurements of electrodes fabricated with ACF-RAW (a), ACF-T05 (b), ACF-T15 (c), and ACF-T25 (d).

3.3. Electrode surface wettability of the prepared electrodes

Though carbon materials have high surface areas, an electrode that cannot contact an aqueous solution is useless for the adsorption of ions [32]. Therefore, it is important to increase the wetted surface of the electrode for improved CDI performance. Accordingly, water drop contact angles of the fabricated electrodes were measured at room temperature to estimate the wettability of the prepared electrode materials [33,34]. Fig. 6 shows images of the contact angles of the untreated ACF and TiO_2-doped ACF electrodes. The contact angles of ACF-RAW, ACF-T05, ACF-T15, and ACF-T25 were approximately 101, 80, 74, and 65°, respectively. The wettability of the electrodes increased as the TiO_2 doping amount increased. These results means that the contact angles decreased with decreasing roughness of the electrodes, even though SEM images for the roughness of electrodes are not provided in this manuscript. Therefore, it was concluded that the surface of the electrodes follows the Cassie-Baxter model [34]. On a Cassie-Baxter surface, liquid is supported by air pockets between grooves if the surface and the contact angle increase with increasing roughness. The high wettability of the prepared electrodes is due to the hydrophilicity of TiO_2, while the untreated ACF electrode had a low wettability due to the hydrophobicity of the carbon surface [14]. The enhanced wettability of the electrodes increases the active sites in the pores as well as the ion transport speed inside the pores [15].

3.4. Electrochemical properties of prepared electrodes

Fig. 7 provides CV curves of the prepared samples at scan rates of 5 and 50 mV s^{-1} in 1 M NaCl solution. At a scan rate of 5 mV s^{-1} (Fig. 7a), all of the cyclic voltammograms exhibited approximately rectangular shapes; this indicates the typical i-E response of carbon materials [33]. At a scan rate of 50 mV s^{-1} (Fig. 7b), the samples exhibited leaf-like shapes, which were mainly due to the ohmic resistance caused by electrolyte motion in the pores of the carbon materials upon formation of an electric double-layer [35]. In addition, no redox peaks were observed in the CV curve of the ACF-RAW electrode; this indicates that the current resulted from electrostatic interactions [36]. Moreover, no redox peaks were observed in the CV curves of the TiO_2-doped ACF electrodes, indicating that no pseudo-faradaic reaction occurred with TiO_2. The specific capacitance (C) of the

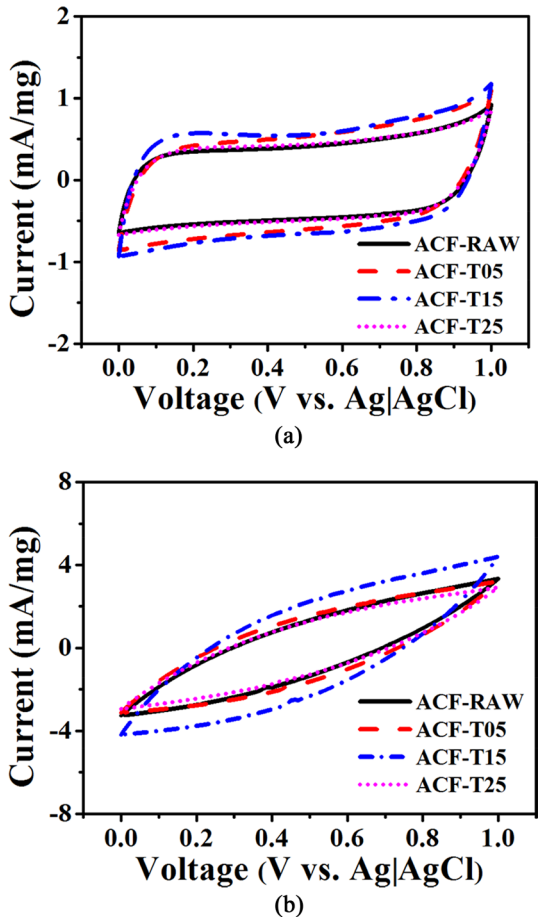

Fig. 7. Cyclic voltammograms of untreated and TiO_2-doped ACF electrodes obtained at scan rates of (a) 5 mV s^{-1} and (b) 50 mV s^{-1}.

electrodes was calculated using the following equation:

$$C = \frac{1}{m\Delta V}\int_0^1 i\,dt \quad (1)$$

, where C (F g^{-1}) is the specific capacitance of the cell, m (g) is the mass of the active material in the working electrode, i (A) is the discharge current for time dt, and ΔV (V) is the potential window of the charge-discharge cycle [29].

The specific capacitances of the samples are listed in Table 3. Although the specific surface area and pore volume decreased upon TiO_2 doping, the specific capacitance values of the ACF-T15 electrode reached 182 and 62 F g^{-1} at scan rates of 5 and 50 mV s^{-1}, respectively, which are 9.6 and 93.8% higher than that value of the ACF-RAW electrode. The TiO_2 particles doped on the ACF surface improved the wettability of the electrodes and reduced the ion-diffusion resistance. Additionally, the electrosorption performance was improved by TiO_2 doping on the ACF surface because the polar TiO_2 groups act as electrosorption sites with improved adsorption strength [37]. However, the specific capacitance of ACF-T25 dramatically decreased compared with that of ACF-RAW. Excessive TiO_2 doping has a negative influence on the specific capacitance because aggregated TiO_2 particles block the pores of ACFs that are ion adsorption sites. If the specific surface area is reduced to more than a certain level, the

Table 3. Specific capacitances of untreated and TiO_2-doped ACF electrodes at different scan rates

Sample	Specific capacitance (F/g)	
	5 mV s^{-1}	50 mV s^{-1}
ACF-RAW	166	32
ACF-T05	171	46
ACF-T15	182	62
ACF-T25	144	40

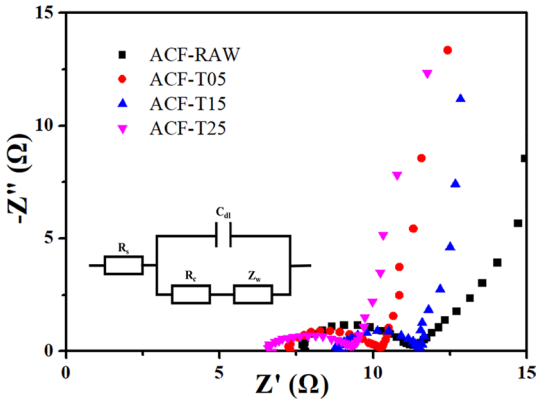

Fig. 8. Nyquist impedance plots of prepared electrodes in 1 M NaCl with frequency ranging from 150 kHz to 0.01 Hz.

specific capacitance is more affected by the specific surface area than by the wettability of electrodes [33].

Fig. 8 presents results of AC impedance measurement of the prepared electrodes. The Nyquist impedance plots of the prepared electrodes correspond to the equivalent circuit for simulation of the impedance spectra shown in Fig. 8, where R_s is the solution resistance, C_{dl} is the double layer capacitance, R_{ct} is the charge transfer resistance, and Z_w is the Warburg diffusion element. The diameter of the semicircle corresponds to R_{ct}. The values of R_{ct} for ACF-RAW, ACF-T05, ACF-T15, and ACF-T25 were calculated and found to be 2.97, 2.12, 1.83, and 1.58 Ω, respectively. The value of R_{ct} also decreased with TiO_2 doping amount. This implies that, as aforementioned, the enhanced wettability facilitated rapid ion transport within ACF pores, which decreased the R_{ct} [15]. At lower frequency, the straight line of the TiO_2/ACF electrodes, which represents the diffusion resistance, has a larger slope than that of the ACF-RAW electrode. This suggests that ion diffusion and migration on the surface of electrode are faster, representing an improved performance of the CDI cell [8]. In conclusion, the introduction of TiO_2 facilitates ion diffusion and migration on the surface of the electrode.

3.5. Desalination performance of prepared electrodes

The CDI performance of the prepared electrodes was investigated to elucidate the effect of TiO_2 doping. Fig. 9 shows conductivity changes of NaCl solutions during the charging step

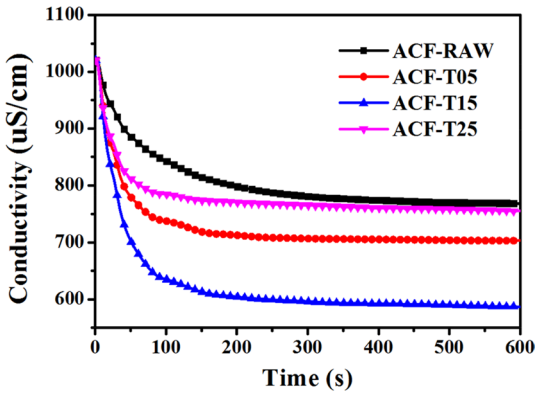

Fig. 9. CDI performance of prepared electrodes in 500 ppm NaCl solution.

in the CDI unit. The conductivity at the initial charging step rapidly decreased, indicating quick adsorption of the salt ions. As time passed, the conductivity slowly decreased and then remained constant once adsorption equilibrium was reached. The minimum conductivity of ACF-T15 was the lowest among the samples. Thus, the CDI performance of ACF-T15 is expected to be improved by TiO_2 doping.

To determine the CDI performance of the prepared electrodes, the salt adsorption capacity and charge efficiency were calculated using Eqs. 2 and 3, respectively. The salt adsorption capacity (Q) was obtained by the change in salt concentration during the charging process:

$$Q = \frac{(\rho_0 - \rho_e)V}{m} \quad (2)$$

where ρ_o (mg L^{-1}) is the initial NaCl concentration, ρ_e is the final NaCl concentration during the adsorption process, V (L) is the total volume of the NaCl solution, and m (g) is the mass of the electrode. The charge efficiency (Λ) was calculated according to Eq. 3:

$$\Lambda = \frac{Q \times F}{\Sigma} = \frac{Q \times F}{\int Idt} \quad (3)$$

where F is the Faraday constant, Q (mol g^{-1}) is the adsorption capacity, and Σ (C g^{-1}) is the electrode charge obtained by integrating the current over time [38]. Fig. 10 shows the salt adsorption capacitance and charge efficiency of the prepared electrodes. The ACF-T15 electrode has the greatest salt adsorption capacity of 10.6 mg g^{-1}, which is 71.9% higher than that of the ACF-RAW electrode. Additionally, the ACF-T15 electrode has the highest charge efficiency of 0.66, which is attributed to the TiO_2 particles on the ACF surface increasing the wettability of the electrodes and thus increasing the active sites of the pores [15]. As seen from the CV results, an increased electrosorption capacity was observed for the TiO_2-doped ACF electrodes, which have highly hydrophilic surfaces due to the Ti-OH groups of TiO_2 [17]. Therefore, the introduction of TiO_2 on the ACF surface is effective for enhancing the CDI performance in terms of the salt adsorption capacity and charge efficiency. Therefore, the TiO_2-doped ACFs prepared by facile ultrasonication-assisted process

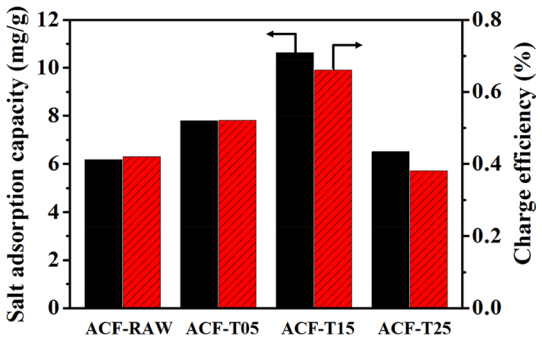

Fig. 10. Salt adsorption capacities and charge efficiencies of prepared electrodes.

have outstanding CDI performance, comparable to that of TiO_2/carbon materials prepared by heat-treatment [13,28,38]. Thus, TiO_2-doped ACFs can be applied as energy efficient electrode materials in the CDI industry.

4. Conclusions

In this study, anatase TiO_2-doped ACFs, as CDI electrode materials, were prepared by a facile ultrasonication-assisted process. The experimental results indicated that anatase TiO_2 particles were successfully and quickly doped on the ACF surface using only an ultrasonication calcining process without heat-treatment. The electrochemical results show that, although the specific surface area and pore volume decreased upon TiO_2 doping, the specific capacitance of the ACF-T15 electrode was much higher than that of the ACF-RAW electrode. In the CDI experiments, the ACF-T15 electrode showed a 71.9% improvement in the salt adsorption capacity over that of the ACF-RAW electrode. This improvement was attributed to the enhanced wettability, which increases the active sites of the pores and facilitates ion transport in the ACF pores. In addition, the Ti-OH groups of the TiO_2-doped ACF electrodes acted as electrosorption sites to increase the electrosorption capacity. Therefore, TiO_2-doped ACF electrodes prepared by the reported facile ultrasonication-assisted process are promising candidates for the practical, industrial application of CDI.

Conflict of Interest

No potential conflict of interest relevant to this article was reported.

Acknowledgements

This work was supported by the Materials and Components Technology Development Program of MOTIE/KEIT (G01201704010267, development of activated carbon fiber materials with very low cost and high functional property for removing sick house syndrome gas).

References

[1] Myint MTZ, Dutta J. Fabrication of zinc oxide nanorods modified activated carbon cloth electrode for desalination of brackish water using capacitive deionization approach. Desalination, **305**, 24 (2012). https://doi.org/10.1016/j.desal.2012.08.010.

[2] Dykstra JE, Zhao R, Biesheuvel PM, van der Wal A. Resistance identification and rational process design in capacitive deionization. Water Res, **88**, 358 (2016). https://doi.org/10.1016/j.watres.2015.10.006.

[3] Shapira B, Avraham E, Aurbach D. Side reactions in capacitive deionization (CDI) processes: the role of oxygen reduction. Electrochim Acta, **220**, 285 (2016). https://doi.org/10.1016/j.electacta.2016.10.127.

[4] Suss ME, Porada S, Sun X, Biesheuvel PM, Yoon J, Presser V. Water desalination via capacitive deionization: what is it and what can we expect from it? Energy Environ Sci, **8**, 2296 (2015). https://doi.org/10.1039/c5ee00519a.

[5] Yao Q, Tang HL. Occurrence of re-adsorption in desorption cycles of capacitive deionization. J Ind Eng Chem, **34**, 180 (2016). https://doi.org/10.1016/j.jiec.2015.11.004.

[6] Huang ZH, Wang M, Wang L, Kang F. Relation between the charge efficiency of activated carbon fiber and its desalination performance. Langmuir, **28**, 5079 (2012). https://doi.org/10.1021/la204690s.

[7] Jung MJ, Jeong E, Kim S, Lee SI, Yoo JS, Lee YS. Fluorination effect of activated carbon electrodes on the electrochemical performance of electric double layer capacitors. J Fluorine Chem, **132**, 1127 (2011). https://doi.org/10.1016/j.jfluchem.2011.06.046.

[8] El-Deen AG, Barakat NAM, Khalil KA, Motlak M, Yong Kim H. Graphene/SnO_2 nanocomposite as an effective electrode material for saline water desalination using capacitive deionization. Ceram Int, **40**, 14627 (2014). https://doi.org/10.1016/j.ceramint.2014.06.049.

[9] Kim J, Byun SC, Chung S, Kim S. Preparation and capacitance properties of graphene based composite electrodes containing various inorganic metal oxides. Carbon Lett, **25**, 14 (2018). https://doi.org/10.5714/CL.2018.25.014.

[10] Tang K, Li Y, Cao H, Su C, Zhang Z, Zhang Y. Amorphous-crystalline TiO_2/carbon nanofibers composite electrode by one-step electrospinning for symmetric supercapacitor. Electrochim Acta, **190**, 678 (2016). https://doi.org/10.1016/j.electacta.2015.12.209.

[11] Li H, Ma Y, Niu R. Improved capacitive deionization performance by coupling TiO_2 nanoparticles with carbon nanotubes. Sep Purif Technol, **171**, 93 (2016). https://doi.org/10.1016/j.seppur.2016.07.019.

[12] Srimuk P, Zeiger M, Jäckel N, Tolosa A, Krüner B, Fleischmann S, Grobelsek I, Aslan M, Shvartsev B, Suss ME, Presser V. Enhanced performance stability of carbon/titania hybrid electrodes during capacitive deionization of oxygen saturated saline water. Electrochim Acta, **224**, 314 (2017). https://doi.org/10.1016/j.electacta.2016.12.060.

[13] Seo MK, Park SJ. Effect of nanosize titanium oxide on electrochemical characteristics of activated carbon electrodes. Curr Appl Phys, **10**, 391 (2010). https://doi.org/10.1016/j.cap.2009.06.032.

[14] Kim C, Lee J, Kim S, Yoon J. TiO_2 sol–gel spray method for carbon electrode fabrication to enhance desalination efficiency of capacitive deionization. Desalination, **342**, 70 (2014). https://doi.

org/10.1016/j.desal.2013.07.016.

[15] Szubzda B, Szmaja A, Halama A. Influence of structure and wettability of supercapacitor electrodes carbon materials on their electrochemical properties in water and organic solutions. Electrochim Acta, **86**, 255 (2012). https://doi.org/10.1016/j.electacta.2012.08.060.

[16] Barai HR, Banerjee AN, Bai F, Joo SW. Surface modification of titania nanotube arrays with crystalline manganese-oxide nanostructures and fabrication of hybrid electrochemical electrode for high-performance supercapacitors. J Ind Eng Chem, **62**, 409 (2018). https://doi.org/10.1016/j.jiec.2018.01.023.

[17] Liu PI, Chung LC, Shao H, Liang TM, Horng RY, Ma CCM, Chang MC. Microwave-assisted ionothermal synthesis of nanostructured anatase titanium dioxide/activated carbon composite as electrode material for capacitive deionization. Electrochim Acta, **96**, 173 (2013). https://doi.org/10.1016/j.electacta.2013.02.099.

[18] Yang K, Zhu J, Zhu J, Huang S, Zhu X, Ma G. Sonochemical synthesis and microstructure investigation of rod-like nanocrystalline rutile titania. Mater Lett, **57**, 4639 (2003). https://doi.org/10.1016/s0167-577x(03)00376-8.

[19] Ghows N, Entezari MH. Ultrasound with low intensity assisted the synthesis of nanocrystalline TiO_2 without calcination. Ultrason Sonochem, **17**, 878 (2010). https://doi.org/10.1016/j.ultsonch.2010.03.010.

[20] Teh CY, Wu TY, Juan JC. An application of ultrasound technology in synthesis of titania-based photocatalyst for degrading pollutant. Chem Eng J, **317**, 586 (2017). https://doi.org/10.1016/j.cej.2017.01.001.

[21] Jung JY, Lee D, Lee YS. CNT-embedded hollow TiO_2 nanofibers with high adsorption and photocatalytic activity under UV irradiation. J Alloys Compd, **622**, 651 (2015). https://doi.org/10.1016/j.jallcom.2014.09.068.

[22] Lee J, Lee B. A simple method to determine the surface energy of graphite. Carbon Lett, **21**, 107 (2017). https://doi.org/10.5714/cl.2017.21.107.

[23] Ryoo MW, Kim JH, Seo G. Role of titania incorporated on activated carbon cloth for capacitive deionization of NaCl solution. J Colloid Interface Sci, **264**, 414 (2003). https://doi.org/10.1016/s0021-9797(03)00375-8.

[24] Li M, Lu B, Ke QF, Guo YJ, Guo YP. Synergetic effect between adsorption and photodegradation on nanostructured TiO_2/activated carbon fiber felt porous composites for toluene removal. J Hazard Mater, **333**, 88 (2017). https://doi.org/10.1016/j.jhazmat.2017.03.019.

[25] Park MS, Ko Y, Jung MJ, Lee YS. Stabilization of pitch-based carbon fibers accompanying electron beam irradiation and their mechanical properties. Carbon Lett, **16**, 121 (2015). https://doi.org/10.5714/cl.2015.16.2.121.

[26] Kim JD, Roh JS, Kim MS. Effect of carbonization temperature on crystalline structure and properties of isotropic pitch-based carbon fiber. Carbon Lett, **21**, 51 (2017). https://doi.org/10.5714/cl.2017.21.051.

[27] Rajagopalan B, Kim B, Hur SH, Chung JS. Alternative binder–free electrode based on facile deposition of carbon/graphene–TiO_2 on the coin cell anode for a lithium–ion battery. Surf Coat Technol, **315**, 359 (2017). https://doi.org/10.1016/j.surfcoat.2017.02.064.

[28] Jia Y, Liu J, Cha S, Choi S, Park YC, Liu C. Magnetically separable Au-TiO_2/nanocube $ZnFe_2O_4$ composite for chlortetracycline removal in wastewater under visible light. J Ind Eng Chem, **47**, 303 (2017). https://doi.org/10.1016/j.jiec.2016.12.001.

[29] Jung MJ, Park MS, Lee YS. Effects of e-beam irradiation on the chemical, physical, and electrochemical properties of activated carbons for electric double-layer capacitors. J Nanomater, **2015**, 240264 (2015). https://doi.org/10.1155/2015/240264.

[30] Jung MJ, Jeong E, Kim Y, Lee YS. Influence of the textual properties of activated carbon nanofibers on the performance of electric double-layer capacitors. J Ind Eng Chem, **19**, 1315 (2013). https://doi.org/10.1016/j.jiec.2012.12.034.

[31] Bagheri S, Mohd Hir ZA, Yousefi AT, Abdul Hamid SB. Progress on mesoporous titanium dioxide: synthesis, modification and applications. Microporous Mesoporous Mater, **218**, 206 (2015). https://doi.org/10.1016/j.micromeso.2015.05.028.

[32] Park BH, Choi JH. Improvement in the capacitance of a carbon electrode prepared using water-soluble polymer binder for a capacitive deionization application. Electrochim Acta, **55**, 2888 (2010). https://doi.org/10.1016/j.electacta.2009.12.084.

[33] Yasin AS, Mohamed HO, Mohamed IMA, Mousa HM, Barakat NAM. Enhanced desalination performance of capacitive deionization using zirconium oxide nanoparticles-doped graphene oxide as a novel and effective electrode. Sep Purif Technol, **171**, 34 (2016). https://doi.org/10.1016/j.seppur.2016.07.014.

[34] Jeong E, Bae TS, Yun SM, Woo SW, Lee YS. Surface characteristics of low-density polyethylene films modified by oxyfluorination-assisted graft polymerization. Colloids Surf A Physicochem Eng Aspects, **373**, 36 (2011). https://doi.org/10.1016/j.colsurfa.2010.10.008.

[35] Lee D, Jung JY, Jung MJ, Lee YS. Hierarchical porous carbon fibers prepared using a SiO_2 template for high-performance EDLCs. Chem Eng J, **263**, 62 (2015). https://doi.org/10.1016/j.cej.2014.10.070.

[36] Jo H, Kim KH, Jung MJ, Park JH, Lee YS. Fluorination effect of activated carbons on performance of asymmetric capacitive deionization. Appl Surf Sci, **409**, 117 (2017). https://doi.org/10.1016/j.apsusc.2017.02.234.

[37] Chen ZL, Sun XW, Guo HF, Song CY. Modified activated carbon electrodes for electrosorption of NaCl from aqueous solution. Adv Mater Res, **113-116**, 2134 (2010). https://doi.org/10.4028/www.scientific.net/AMR.113-116.2134.

[38] El-Deen AG, Choi JH, Kim CS, Khalil KA, Almajid AA, Barakat NAM. TiO_2 nanorod-intercalated reduced graphene oxide as high performance electrode material for membrane capacitive deionization. Desalination, **361**, 53 (2015). https://doi.org/10.1016/j.desal.2015.01.033.